Volume 16
Number 13
7 April 2024
Pages 6317-6762

Nanoscale

rsc.li/nanoscale

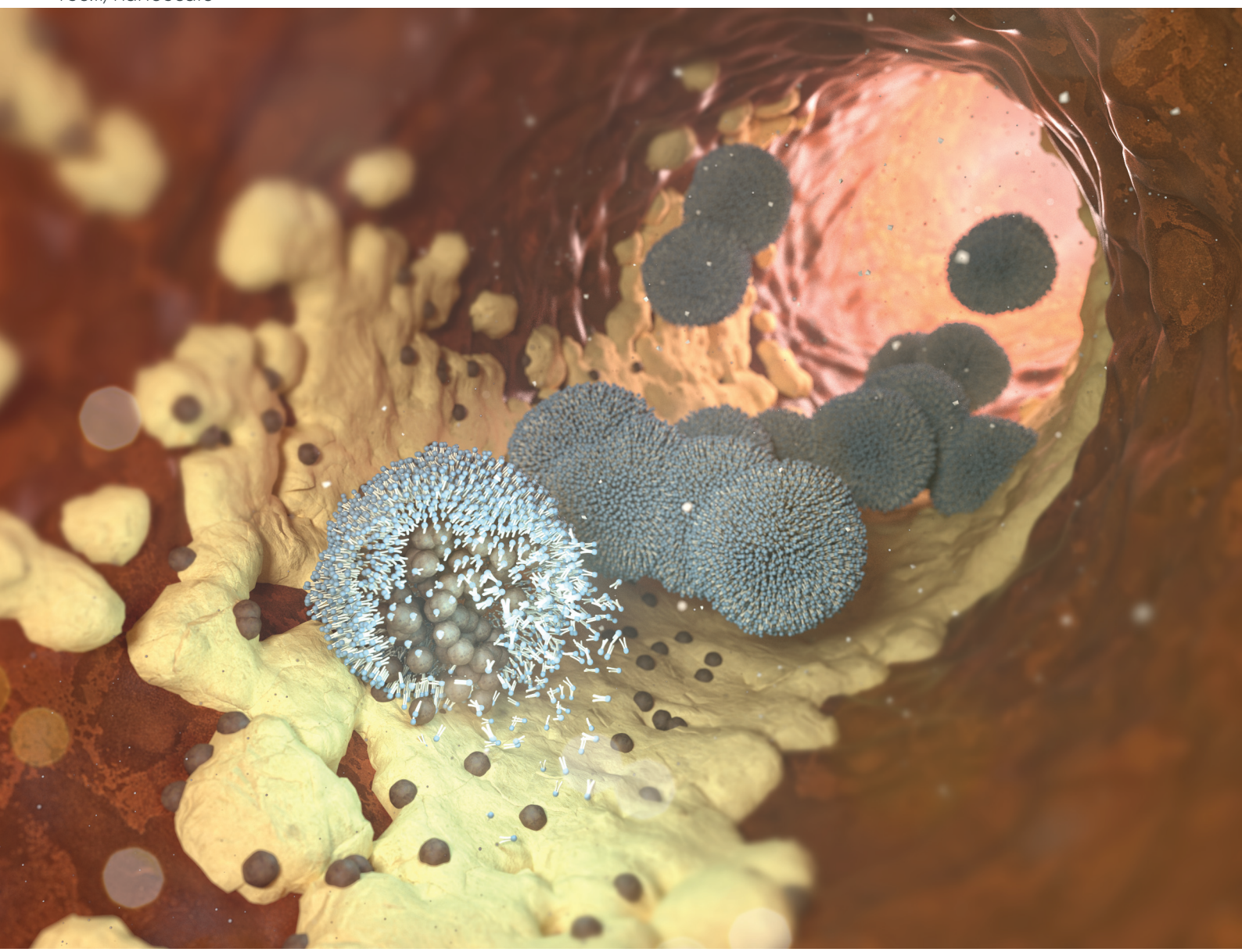

ISSN 2040-3372

ROYAL SOCIETY OF CHEMISTRY

PAPER
Jacob F. Bentzon, Fernando Herranz *et al.*
Sphingomyelinase-responsive nanomicelles for targeting atherosclerosis

NCNST

Nanoscale

PAPER

View Article Online
View Journal | View Issue

Cite this: *Nanoscale*, 2024, **16**, 6477

Sphingomyelinase-responsive nanomicelles for targeting atherosclerosis

María Muñoz-Hernando,[a,b] Paula Nogales,[b] Irene Fernández-Barahona,[a] Jesús Ruiz-Cabello,[d,e,f,g] Jacob F. Bentzon*[b,c] and Fernando Herranz *[a,g]

Received 20th December 2023,
Accepted 23rd February 2024

DOI: 10.1039/d3nr06507c

rsc.li/nanoscale

Atherosclerosis, a leading cause of cardiovascular diseases requires approaches to enhance disease monitoring and treatment. Nanoparticles offer promising potential in this area by being customisable to target components or molecular processes within plaques, while carrying diagnostic and therapeutic agents. However, the number of biomarkers available to target this disease is limited. This study investigated the use of sphingomyelin-based nanomicelles triggered by sphingomyelinase (SMase) in atherosclerotic plaques. Accumulation of iron oxide-based nanomicelles in the plaque was demonstrated by fluorescence, MR imaging and electron microscopy. These findings demonstrate the possibility of utilising SMase as a mechanism to retain nanoprobes within plaques, thus opening up possibilities for future therapeutic interventions.

Introduction

Atherosclerosis remains the primary cause of cardiovascular diseases globally, and new approaches are needed to identify at-risk patients, monitor disease progression, and improve therapies. To be part of future solutions nanoparticles can be engineered to target specific constituents or molecular processes in atherosclerotic plaques and can carry both diagnostic and therapeutic agents, thereby potentially delivering both improved disease monitoring and targeted therapies. Previous studies have used nanoparticles to target different types of structures in atherosclerotic plaques, mainly through the conjugation of nanoparticles with antibodies or small molecules capable of binding to macrophages,[1,2] microcalcifications,[3] oxLDL,[4] and adhesion molecules,[5] among others.[6] Other approaches have used nanoparticles designed such that their physicochemical properties can selectively accumulate the cargo in atherosclerotic plaques. Given that targeting moieties such as antibodies are cumbersome and expensive to produce in large amounts, the latter approach renders higher scalability, and we reasoned that selectivity for atherosclerosis may still be achieved if the surface of the particles is designed to hijack endogenous retention mechanisms in the atherosclerotic plaque. Atherosclerosis is driven by the accumulation of cholesterol-rich apolipoprotein B (ApoB)-containing lipoproteins, predominantly in the form of low-density lipoproteins (LDLs),[7] in the arterial intima. Once retained, lipoproteins are modified and the altered lipoprotein surfaces are recognised by and activate the innate and adaptive immune systems. In this manner, the continuous influx of atherogenic lipoproteins fuels a chronic low-level inflammatory state that drives plaque development. Enzymes play an important role in retaining incoming LDL particles in the established atherosclerotic plaque.[8,9] Among the different arterial enzymes with this function, secretory sphingomyelinase (SMase), which hydrolyses sphingomyelin molecules present in the surface of LDL particles into ceramide, has been shown to be particularly important in atherosclerosis progression. SMase and similar enzymes have been proposed as targets of interest for the development of novel treatments.[10] Genetic deletion of this enzyme in hypercholesterolaemic animals drastically retards atherosclerotic plaque development.[11] Furthermore, several *in vitro* and *in vivo* studies have shown that aggregation-prone human LDLs are enriched in sphingomyelin and ceramide, and contain fewer choline phospholipids than aggregation-resistant LDLs.[12]

In the present study, we show that SMase can be exploited as an endogenous workhorse to accumulate nanoprobes in atherosclerotic plaques. We designed sphingomyelin-based

[a]*Grupo de Nanomedicina e Imagen Molecular, Instituto de Química Médica (IQM/CSIC), Juan de la Cierva 3, 28006 Madrid, Spain. E-mail: fherranz@iqm.csic.es*
[b]*Centro Nacional de Investigaciones Cardiovasculares, CNIC, Melchor Fernández-Almagro 3, 28029 Madrid, Spain*
[c]*Department of Clinical Medicine, Aarhus University, Denmark*
[d]*CIC biomaGUNE, Basque Research and Technology Alliance (BRTA), Paseo de Miramon 182, 20014 Donostia San Sebastián, Spain*
[e]*Ikerbasque, Basque Foundation for Science, Plaza Euskadi 5, 4800 Bilbao, Spain*
[f]*NMR and Imaging in Biomedicine Group, Department of Chemistry in Pharmaceutical Sciences, Pharmacy School, University Complutense Madrid, 28040 Madrid, Spain*
[g]*CIBER Enfermedades Respiratorias (CIBERES), Melchor Fernández-Almagro 3, 28029 Madrid, Spain*

nanomicelles carrying a cargo of iron oxide particles and found that they can be destabilised by SMase *in vitro* and accumulate in murine atherosclerotic plaques after intravenous injection, as documented by fluorescence tracking, MR imaging, and electron microscopy.

Methods

Synthesis of oleic acid coated iron oxide nanoparticles (OAIONPs)

The oleic acid iron oxide (Fe_3O_4) nanoparticles (OAIONPs) were synthesised using iron acetylacetonate as the precursor and phenyl ether as the solvent. A mixture of $Fe(acac)_3$ (1.42 g, 4 mmol), 1,2-hexadecanediol (4.8 g, 20 mmol), oleic acid (3.38 g, 12 mmol), oleylamine (3.2 g, 12 mmol), and diphenyl ether (40 mL) was added to a round three-neck flask (100 mL). The reaction mixture was heated under mechanical stirring and a flow of nitrogen gas up to a temperature of 200 °C, which was maintained for 120 min. The solution was then heated under reflux up to 250 °C for 30 min with a nitrogen balloon on top of the condenser. Subsequently, the solution was cooled down to room temperature (r.t.) and 30 mL of 96% ethanol (EtOH) were added. The resulting solution was placed under a neodymium (Nd–Nb–B) magnet for 10 min. During this time, the most superparamagnetic nanoparticles precipitated towards the magnet while the less magnetic ones were eliminated with the remaining supernatant. Following this step, 20 mL EtOH were added to the mixture and the solution was sonicated (Branson 250, 42 ± 6 kHz) for 10 min to resuspend the precipitated nanoparticles. This purification step was repeated five more times and after the last purification the nanoparticles where resuspended in 30 mL of hexane.

Synthesis of sphingomyelin iron oxide nanomicelles (SPHIONMs)

For the synthesis of sphingomyelin iron oxide nanomicelles (SPHIONMs), sphingomyelin (SPH) (57 mg, 0.07 mmol) was first dispersed in 15 mL of PBS. Once the lipid was dissolved, a 1 mL aliquot of the OAIONPs (10 mg Fe per mL), dispersed in hexane, was added to the solution and the resulting mixture was sonicated under robust stirring for 20 min at 37 °C. The nanoemulsion was kept under sonication for another 60 min to evaporate all traces of hexane, resulting in the formation of a homogenous aqueous solution. Finally, aggregates were removed by filtration (0.45 μm Milex HV-filter). The same protocol was used for the preparation of 1,1′-dioctadecyl-3,3,3′,3′-tetramethylindocarbocyanine perchlorate (DiIC18(5)) labelled SPHIONMs except that 1 mg of the fluorophore, dissolved in hexane, was added to the solution at the same time as the OAIONPs. In addition, polysorbate 80 (P80) coated IONMs were produced, as the control nanomicelles for SPHIONMs experiments. For this purpose, the same protocol was followed except that SPH was substituted by 150 mg (0.11 mmol) of P80.

Physicochemical characterisation

Dynamic light scattering (DLS). The hydrodynamic size, polydispersity index (PDI), and zeta potential of all the synthesised NPs was measured by dynamic light scattering (DLS) (Zetasizer Nano ZS90, Malvern Instruments, Malvern, UK). All measurements were performed at r.t. and in triplicates. In addition, DLS was used to assess the colloidal stability of the NPs, by monitoring the changes in their hydrodynamic size and PDI with time, and after their incubation with PBS.

Transmission electron microscopy (TEM). The morphology and the core size of the NPs were determined by transmission electron microscopy (TEM, $N = 50$). TEM analyses were carried out at the National Center of Electron Microscopy of the Universidad Complutense de Madrid (Madrid, Spain). For the magnetic NPs (SPHIONMs and cit-IONPs), a drop of diluted NP sample was placed on top of a carbon-coated copper grid and observed under TEM using a 200 keV JEOL-2000 FXII instrument (Jeol Ltd, Tokyo, Japan).

Fourier transform infrared spectroscopy (FT-IR). Fourier transform infrared spectroscopy (FT-IR) spectra were obtained for the SPHIONMs on a PerkinElmer Spectrum 400 Series spectrometer (PerkinElmer, USA); each spectrum was obtained by averaging 32 interferograms with a resolution of 1 cm^{-1}.

Thermogravimetric analysis (TGA). Thermogravimetric analysis (TGA) spectra of the SPHIONMs were obtained with a Seiko TG/ATD 320 U, SSC 5200 spectrometer (Seiko Instruments, Chiba, Japan) at the Universidad Autónoma de Madrid (Institute of Materials Science, Madrid, Spain). For this purpose, SPHIONMs were lyophilised, and the dried sample was heated from 20 °C to 1000 °C at 10 °C min^{-1} under a 100 mL min^{-1} air flow.

Relaxometry. The longitudinal (T_1) and transverse (T_2) relaxation times of SPHIONMs at different concentrations were measured using a relaxometer at 1.5 T and 37 °C (Bruker MQ60, Bruker Biospin, Germany). The obtained relaxation rates ($R_1 = 1/T_1$, $R_2 = 1/T_2$) were then plotted against their corresponding iron concentration values, to obtain the relaxivity values of the SPHIONMs.

In vitro degradation of SPHIONMs with sphingomyelinase

The *in vitro* degradation of SPHIONMs in the presence of sphingomyelinase (SMase) was assessed by measuring the changes in the hydrodynamic size of the nanomicelles after their incubation with the enzyme. To this end, a solution of SPHIONMs (1.5 mL) mixed with SMase (0.2 U) was incubated at 37 °C and the hydrodynamic size and PDI of the sample was measured, by DLS (Zetasizer Nano ZS90, Malvern Instruments, UK), at different time points (from 5 to 180 min). In addition, a solution containing only the SPHIONMs was also incubated at 37 °C, and their hydrodynamic size and PDI was measured as a control.

Animal models

Animal experiments were approved by the ethical review boards at CNIC and Universidad Autónoma and permitted by

the Comunidad de Madrid (PROEX 266/16 and PROEX 265/16). Furthermore, all experiments followed the 3R principles to include the minimum number of animals required for sufficient statistical power. All compared mice were littermates, housed together, and subjected to the same procedures. *Ldlr*$^{-/-}$ mice (B6.129S7-Ldlr^{tm}1Her/J, the Jackson Laboratory) were used to study the accumulation of SPHIONMs in plaques by confocal microscopy and non-invasive imaging. *Ldlr*$^{-/-}$ mice have elevated plasma cholesterol level and develop atherosclerosis slowly on standard laboratory diet.[13] On high-fat diets, they have very high plasma cholesterol levels and fast development of atherosclerotic plaques.[13]

In this work, advanced lesions were induced by feeding the mice for 24 weeks with high-fat diet (S9167-E011, Sniff). Only female mice were used.

In vivo MRI

For the atherosclerosis detection T_2-weighted MRI experiments, a baseline scan was acquired before SPHIONMs injection. Following this, mice were intravenously injected with SPHIONMs (0.38 mg Fe per mL 150 μL), and 24 h after nanomicelle injections MRI scans were acquired using the same sequence. All MRI experiments were performed on a 7 T Bruker Biospec 70/30 USR MRI system (Bruker Biospin GmbH, Ettlingen, Germany). Anesthesia was induced with 3% isoflurane in 30% oxygen and maintained 1–2% isoflurane along the experiment. Animals were positioned in a customised 3D printed bed with a head holder and kept warmed with heated air pumped through an MRI compatible system interfaced to a Monitoring and Gating Model 1025 (SA instruments). Temperature control (anal) and respiration (through a respiratory pad) were registered along the experiment. To ensure an accurate positioning, pure axial and four-chamber view scout images were used to set up the representative aortic arch view. From these, 19 × 21 mm^2 images were obtained between the brachiocephalic artery and left common carotid artery, perpendicular to the direction of the flow in the aorta, with a self-gated CINE spoiled gradient echo (ig-FLASH). Acquisition and reconstruction voxel size: 0.11 × 0.11 mm^2, slice thickness 0.8 mm. Additional acquisition details are: echo time TE = 6.0 ms, repetition time TR = 9.8 ms, flip angle FA = 10°, 1 average. T_2-Weighted MRI images were analysed quantitatively by measuring signal intensities in the aortic wall before and after nanomicelle injection, for both SPHIONM and P80IONM injected mice. To that end, aortic wall ROIs (N = 10 for each mouse) were manually drawn.

Confocal microscopy

Confocal microscopy was used to study the accumulation of the fluorescent SPHIONMs. In atherosclerotic lesions. All fluorescent cross-sections were analysed with a Leica TCS SP5 microscope (Leica, Wetzlar, Germany) using either a HCX PL APO lambda blue 20×/0.7 multi-immersion objective or a HCX PL APO CS 40×/1.25 oil objective. Leica LAS X software was used for image acquisition. The acquisition method was kept constant for every cross-section so that comparisons between images could be performed.

Tissue transmission electron microscopy

The ascending part of the aorta and a piece of liver of *Ldlr*$^{-/-}$ mice were sent for TEM imaging. For tissue processing, after perfusion, the arteries and the livers were cut into approximately 3 mm pieces and fixed for 6 hours in 2.5% glutaraldehyde and 4% paraformaldehyde in a 0.1 M phosphate buffer (pH 7.3). Afterwards, samples were rinsed in ice-cold phosphate buffer. Tissues were post-fixed in 1% aqueous osmium tetroxide for 1 hour. They were washed with distilled water, dehydrated in a graded series of acetone, and finally embedded in Spurr's resin (TAAB laboratories, Aldermaston Ward, UK). Ultrathin sections (60 nm) were cut with an ultramicrotome Leica ultracut E, (Leica, Wetzlar, Germany), mounted on 200 mesh copper grids, and finally stained with uranyl acetate 2% and Reynold's lead citrate. Electron micrographs were obtained using a Jeol 1400 plus (Jeol Ltd, Tokyo, Japan) operated at 100 kV and equipped with a CCD camera Gatan SC ORIUS 200 (Gatan, Pleasanton, USA).

Statistical analysis

Statistical tests were performed in Prism 8 (GraphPad Software). Two-sample comparisons were analysed by the unpaired Student's t-test for normally distributed data and by Mann–Whitney test for non-normally distributed data. Three or more samples' comparisons were performed with the ordinary one-way ANOVA test for normally distributed data and by the Kruskal–Wallis test for non-normally distributed data. Variance between samples was calculated using F-test. Bars in scatter dot plots represent mean ± SD.

Results

Synthesis and characterisation of sphingomyelin-coated iron oxide nanomicelles

In this study, we synthesised water-stable sphingomyelin iron oxide nanomicelles (SPHIONMs). These nanomicelles were composed of hydrophobic iron oxide nanoparticles (IONPs) arranged in the core and stabilised by sphingomyelin (SPH) molecules. Our working hypothesis was that the enzymatic activity of arterial sphingomyelinase (SMase) on the polar head of SPH molecules causes the destabilisation and degradation of SPHIONMs, thereby facilitating the accumulation of hydrophobic IONPs within atherosclerotic plaques. This, in turn, enables detection using magnetic resonance imaging (MRI). The SPHIONMs were prepared using a two-step nanoemulsion synthetic protocol based on a method previously developed by our group.[14] First, we synthesised hydrophobic oleic acid-coated iron oxide nanoparticles (OA-IONPs) by the thermal decomposition of the iron precursor, iron acetylacetonate, in the presence of oleic acid, oleylamine, and 1,2-hexadecanediol. The obtained OA-IONPs showed a narrow size distribution, with a core size of 7.0 ± 1.4 nm, a hydrodynamic size of 13.0 ±

3.5 nm and a polydispersity index (PDI) of 0.16 ± 0.02, as measured by TEM and DLS, respectively (Fig. 1a and b). Subsequently, a nanoemulsion method was used to produce physiologically viable nanoparticles. The OA-IONPs were encapsulated in a sphingomyelin layer to form the nanomicelles. Using this procedure, water-stable nanomicelles with a narrow size distribution (PDI = 0.17 ± 0.02), a hydrodynamic size of 73.7 ± 4.2 nm and a zeta potential value of −7.3 ± 1.5 mV were produced. The reproducibility of the nanoemulsion method was excellent, with no visible changes in the hydrodynamic size distributions of the three SPHIONM batches (Fig. 1a). Furthermore, TEM analysis of the SPHIONMs revealed the presence of several OA-IONPs (~7 nm) grouped together, forming an iron oxide core of approximately 40 nm (Fig. 1c). This structure is typically observed for iron oxide nanomicelles.[14]

The same protocol was employed to prepare nanomicelles for fluorescence-based imaging, except that 1 mg of fluorophore DilC18(5) was added to the nanoemulsion formulation. Fluorescently labelled nanomicelles did not show any significant changes compared to non-labelled micelles. A similar protocol using polysorbate 80 as the hydrophilic coating was used to prepare control nanomicelles (P80IONMs). The characterisation of this type of nanomicelles was previously described by our group, and studies have shown that P80IONMs do not accumulate in murine atherosclerotic lesions.[14]

Several SPHIONM batches were synthesised to validate the reproducibility of the process. The composition of SPHIONM was analysed using inductively coupled plasma mass spectrometry (ICP), Fourier-transform infrared spectroscopy (FTIR), and thermogravimetric analysis (TGA).

FTIR spectra showed characteristic bands for the SPH structural moiety, including bands in the ranges of 1600–1700 cm^{-1} (C═O), 1480–1580 cm^{-1} (C–N and N–H), which were superimposed on the typical signal of oleic acid magnetite NPs,[15,16] and bands in the ranges of 1200–1300 cm^{-1} (phosphodiester band, P═O) and 1000–1100 cm^{-1} (C–C). The spectra were similar for all the analysed samples (Fig. 1e). TGA results showed that for all samples, the organic coating (including OA and SPH) degraded from 200 to 450 °C, representing approximately 25% of the total weight of the nanomicelles. This low weight suggests that a very thin layer of SPH molecules is intercalated with the fatty chains of OA (Fig. 1f). Furthermore, iron concentration was similar in all the samples, 0.38 ± 0.05 mg Fe per mL SPHIONM as determined by ICP.

Further characterisation was performed to prepare for the *in vivo* experiments. First, stability in PBS at 37 °C was studied at different time points. Fig. 1d shows that the SPHIONMs maintained a stable hydrodynamic size throughout the incubation process. In addition, the relaxometric parameters of the SPHIONM were studied at 1.5 T and 37 °C (Fig. 1g and h). Results showed the expected behaviour of superparamagnetic nanoparticles with a low r_1 value of 1.98 mM^{-1} s^{-1} and a high r_2 value of 125.90 mM^{-1} s^{-1}, giving a high r_2/r_1 ratio of 63.5 indicating that SPHIONM could be used as a contrast agent for

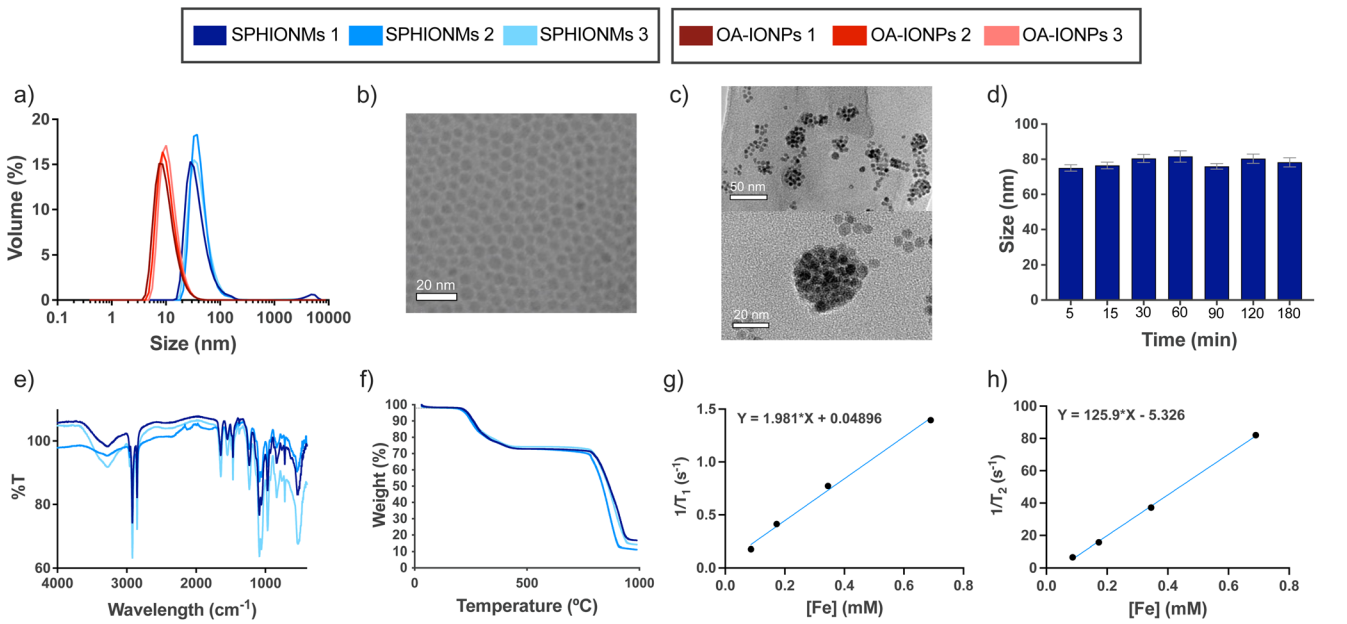

Fig. 1 Physicochemical characterisation of SPHIONMs. (a) Hydrodynamic size distributions of three different batches of OA-IONPs and SPHIONMs determined by DLS. (b) TEM image of the OA-IONP solution; scale bar: 20 nm. (c) TEM of an SPHIONM solution (top), higher magnification image of a single nanomicelle (bottom); scale bars, 50 nm and 20 nm, respectively. (d) Hydrodynamic size (*z*-average, mean ± SD) of SPHIONMs in 1× PBS from t = 0 to t = 180 min (slope of linear trend with time not significantly different from 0 p = 0.13). (e) FTIR spectra of three different batches of SPHIONMs. (f) Thermogravimetric curves for three batches of SPHIONMs. (g) Longitudinal relaxivity and (h) transversal relaxivity in mM^{-1} s^{-1} for SPHIONMs at 37 °C and 1.5 T. OA: oleic acid; SPH: sphingomyelin.

Table 1 Summary of SPHIONM characterisation. Values indicate mean ± SD

Hydrodynamic size (nm)	Core size (nm)	PDI	*Z*-potential (mV)	r_1 (mM^{-1} s^{-1})	r_2 (mM^{-1} s^{-1})	r_1/r_2	[Fe] (mg mL^{-1})
74 ± 4.2	40	0.17 ± 0.02	−7.3 ± 1.5	1.98	125.9	63.5	0.38 ± 0.05

T_2-weighted MRI. The main physicochemical parameters for SPHIONMs are shown in Table 1.

In vitro degradation by sphingomyelinase

Our hypothesis was based on the potential destabilisation of SPHIONMs in the presence of SMase. To demonstrate whether SMase had this effect on the nanomicelles, an *in vitro* study was performed. For this purpose, SPHIONMs were incubated with a known concentration of SMase at 37 °C, and their behaviour over time was studied using DLS. The results showed an increase in the percentage of SPHIONMs with a large hydrodynamic size and a consequent increase in the PDI of the solution (from 0.1 to 0.9) (Fig. 2a).

In addition, their *z*-average by volume showed an abrupt rise as soon as 30 min after incubation with the enzyme, while no change was observed in the nanomicelles incubated under the same conditions without SMase (Fig. 2b). Furthermore, a simple visual inspection confirmed this large aggregation, as shown in Fig. 2c, where the initially stable colloidal dispersion of the SPHIONMs rapidly became turbid with visible precipitates.

In vivo biodistribution study

After characterising the stability of the SPHIONMs in PBS and their *in vitro* behaviour in the presence of SMase, we moved on to the *in vivo* experiments. First, we studied the biodistribution and MRI signal of the nanomicelles. For this purpose, 150 μL of the SPHIONM solution (0.38 mg Fe per mL) were injected by i.v. tail injection into healthy C57BL/6 mice (N = 5, 18 weeks old).

Given the size of SPHIONMs, we expected clearance through the liver; therefore, MR scans of the murine livers were performed before and 30, 60, and 90 min after nanomicelle injection. Imaging studies showed that SPHIONMs started accumulating in the liver approximately 30 min after nanomicelle injection, showing a clear decrease in signal with time (Fig. 3). These results further confirmed the ability of SPHIONMs to behave as a contrast agent for T_2-weighted MRI *in vivo*. Similarly, we observed a strong uptake in the spleen and liver but not in the lungs and kidneys, after the intravenous injection of fluorescently labelled SPHIONMs.

Atherosclerosis detection experiments

Once it was confirmed that SPHIONMs could produce a hypointense signal on T_2-weighted MRI, we proceeded to validate their ability to accumulate in atherosclerotic lesions due to the presence of SMase. For this purpose, $Ldlr^{-/-}$ mice were fed a high-fat diet from 8 to 32 weeks of age to induce atherosclerosis. Nanomicelle accumulation was first studied *in vivo* using MR imaging; following this, mouse tissues were collected for *ex vivo* analysis using confocal microscopy and TEM. The experimental design of these studies is shown in Fig. 4a.

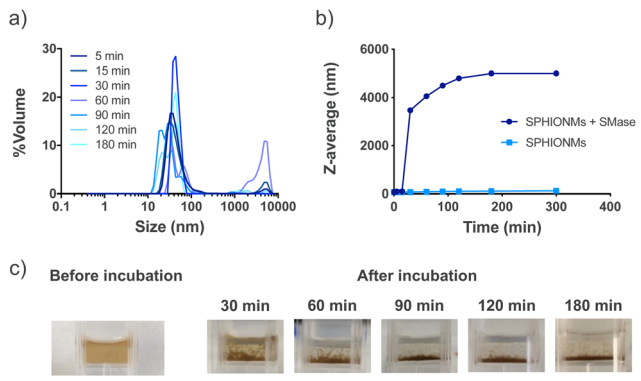

Fig. 2 *In vitro* degradation of SPHIONMs by SMase. (a) Changes in the hydrodynamic size distribution of the SPHIONM solution incubated with sphingomyelinase from t = 5 to t = 180 min. (b) Changes in *z*-average of SPHIONM solutions incubated with or without sphingomyelinase from t = 5 to t = 180 min. The experiments were performed at 37 °C in PBS and were repeated twice. (c) Visual evaluation of SPHIONMs aggregation after incubation with sphingomyelinase.

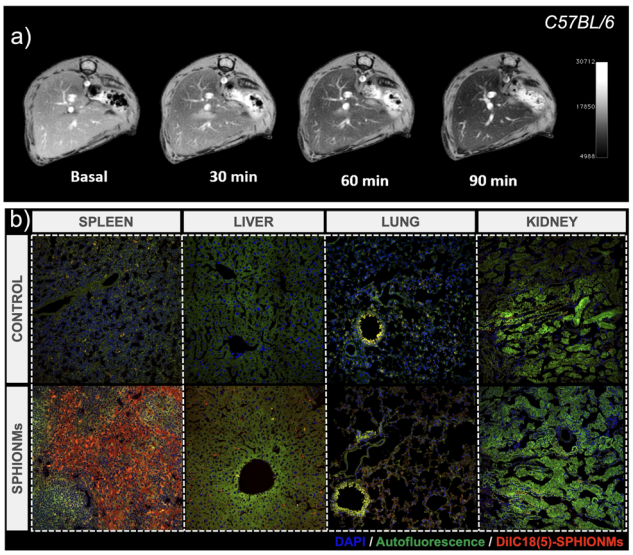

Fig. 3 (a) *In vivo* T_2-weighted MRI biodistribution study. Representative liver MR images of C57BL/6 mice (18 weeks old) before (basal), and 30, 60, and 90 min after injection of SPHIONMs (0.38 mg Fe per ml, 150 μL). (b) Confocal microscopy images of control organs and organs after i.v. injection of fluorescently labelled SPHIONMs in C57BL/6 mice (18 weeks old).

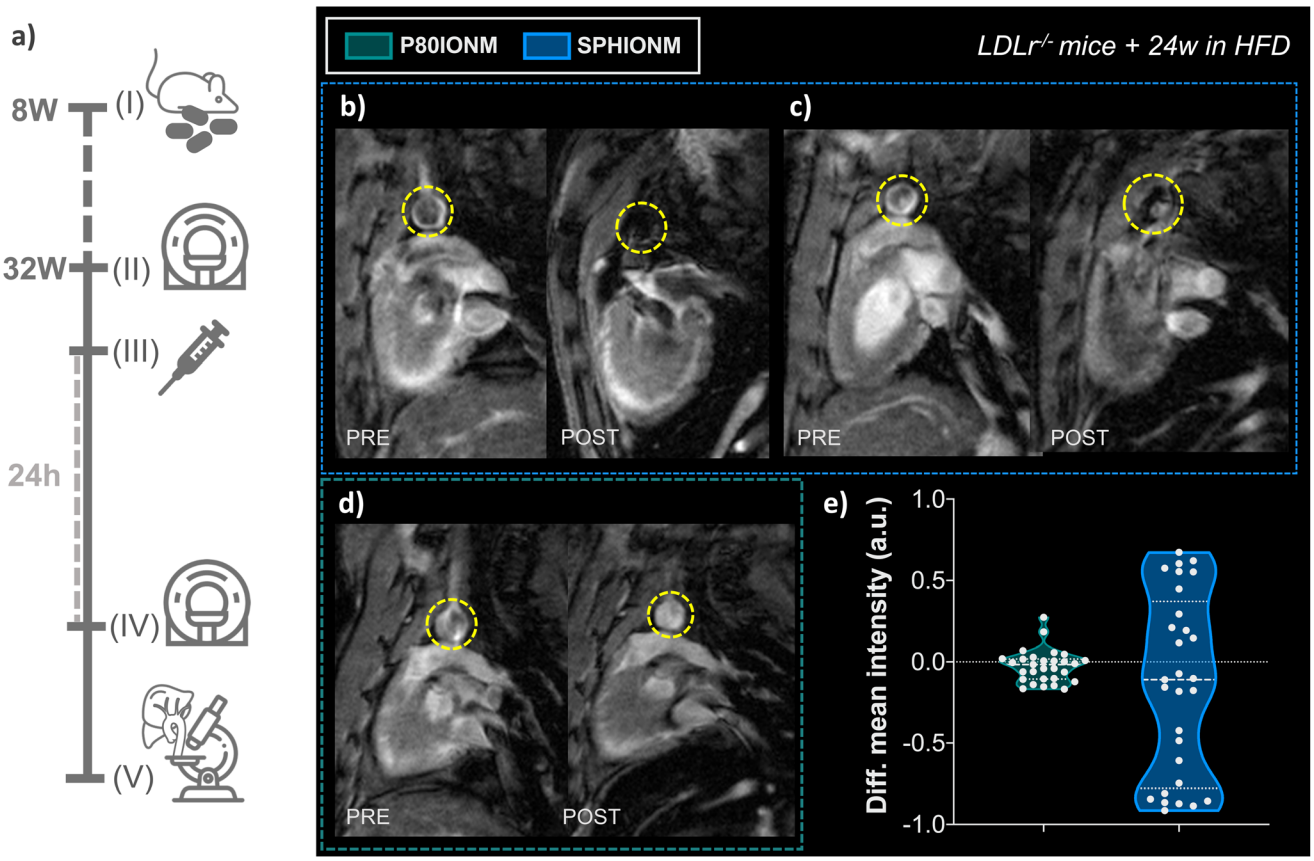

Fig. 4 (a) Experimental design for atherosclerosis detection using SPHIONMs. (I) Animal model preparation. *Ldlr*$^{-/-}$ mice (8 weeks old) were fed on HFD diet for 24 weeks for atherosclerosis induction. (II) Baseline *in vivo* T_2-weighted MRI. Baseline T_2-weighted MRI cardiac scans, focused on the aortic arch of the animals, were acquired in atherosclerotic *Ldlr*$^{-/-}$ mice (32 weeks old) (N = 6). (III) Nanomicelle injection. After image acquisition, mice were injected intravenously with fluorescent-labelled SPHIONM (150 μL) (N = 5) or fluorescent-labelled control P80IONMs (150 μL) (N = 4). (IV) *In vivo* T_2-weighted MRI. After 24 h, T_2-weighted cardiac MRI scans focused on the aortic arch of the animals were acquired using the same MR sequence. Animals were euthanised after image acquisition by exsanguination and perfusion-fixed. (V) *Ex vivo* analysis. Organs were collected for *ex vivo* analysis using confocal microscopy and TEM. (b–e) *In vivo* T_2-weighted MRI studies for atherosclerosis detection. Representative MR images of the heart and aorta of *Ldlr*$^{-/-}$ mice with atherosclerosis induced by 24 weeks of HFD. Panels show scans obtained before and 24 hours after injection of (b–c) SPHIONMs (0.38 mg Fe per mL, 150 μL) (N = 3) and (d) P80IONMs (0.41 mg Fe per mL, 150 μL) (N = 3). Yellow circles indicate the aortas. (e) Differences in the mean intensity at the arterial wall in *Ldlr*$^{-/-}$ mice injected with P80IONM or SPHIONM. Values were acquired from manually drawn aortic wall ROIs (N = 10 per mouse). The variances between the two groups were significantly different (****p < 0.0001, as obtained from the F-test).

In vivo T_2-weighted MRI

First, we studied the accumulation of nanomicelles in atherosclerotic lesions using *in vivo* T_2-weighted MR. For plaque visualisation, an MRI scan focused on the aortic arch of the animals was performed before (baseline) and 24 h after nanomicelle injection to characterise the intensity differences in the aorta. Imaging studies were carried out in mice injected with SPHIONM (0.38 mg Fe per mL) (N = 3) and control mice injected with P80IONM (0.41 mg Fe per mL) (N = 3). Following the MRI scans, mice were euthanised and perfusion-fixed, and their aortas and livers were collected and processed for *ex vivo* TEM and confocal microscopy analysis. Representative images of the acquired T_2-weighted MRI scans are shown in Fig. 4b–d. Differences in the signal intensity of the aorta were observed between the scans performed before and after the injection of SPHIONMs. T_2-Weighted images obtained 24 h after SPHIONM injection clearly showed hypointenses areas in several some aortic areas. In these areas, the structure of the arterial wall that was visible on T_2-weighted baseline scans seemed to "disappear". These results suggested the presence of SPHIONMs. Importantly, this effect was not observed in the T_2-weighted MRI scans of mice injected with the control P80IONMs (Fig. 4d). Furthermore, a hypointense effect was observed in the livers of all animals, both SPHIONM- and P80IONM-injected mice, confirming that the absence of a negative signal in the aorta of control mice was not due to injection errors.

To quantify the observations, signal intensities in the aortic wall were measured before and after injection of the two types of nanomicelles. Measurements obtained from ROIs in slices of the aortic arch (N = 10 per mouse, 3 mice per group)

showed a decreasing trend in the mean intensity of the aortic wall after SPHIONM injection. However, these differences were not statistically significant. Furthermore, no significant differences were found after the injection of P80IONM. Given that the aortic wall mean intensity after SPHIONM injection was only slightly lower, we plotted the variation between the mean intensity values before and after injection of nanomicelles for each analysed ROI (Fig. 4e). The results showed that, after the injection of P80IONM, there was almost no variation in the mean intensity values, whereas in the case of the SPHIONMs, a high variation was shown for most of the ROIs, indicating changes in the magnetic activity of the area, further suggesting nanomicelle accumulation.

Confocal microscopy

To confirm that the signal changes in T_2-weighted MRI studies were produced by nanomicelle accumulation, the aortas of the *Ldlr*$^{-/-}$ mice were extracted and sectioned to study nanomicelle accumulation in the atherosclerotic plaque *ex vivo* using confocal microscopy.

Images of sections of the inner arch of the ascending aorta, an atheroprone site,[17] were acquired using fixed settings for acquisition and image processing. Sections from mice injected with fluorescent SPHIONMs and fluorescent P80IONMs were analysed and compared.

The results showed a clear accumulation of fluorescent SPHIONMs in the atherosclerotic plaques (Fig. 5a). This accumulation was shown to be higher in the luminal part of the plaque, particularly in the plaque shoulders. Importantly, no accumulation of fluorescent control P80IONMs was observed in the control mice (Fig. 5b). These results further confirmed the ability of SPHIONMs to accumulate in atherosclerotic plaques, while also indicating the specificity of the nanoprobe, as no accumulation was observed with the P80IONMs.

Transmission electron microscopy

To confirm the *in vivo* accumulation of SPHIONMs in atherosclerotic lesions, *ex vivo* TEM studies were performed on aortic and liver tissues extracted from *Ldlr*$^{-/-}$ mice injected with SPHIONMs.

Due to the extremely high magnification and small field of view of TEM, we could not observe the whole plaque simultaneously. Therefore, prior to imaging of the aortic tissues, liver sections from the same mice were analysed. Given that SPHIONM are eliminated through the liver, as shown by the MRI studies, we expected to find a higher amount of nanomicelles in those tissues, allowing us to identify SPHIONMs in an easier manner.

Results from the liver sections showed the presence of nanomicelle-like structures inside the liver cells (Fig. 6b). Higher magnification images allowed us to identify clusters of aggregated OA-IONPs. As it can be observed, these structures resemble those observed in the TEM images of the SPHIONM solutions (Fig. 6a). Once we were able to identify SPHIONMs, we acquired TEM images of the inner arch of the ascending aorta. Images from these sections also showed the presence of SPHIONMs in the plaque cells closer to the lumen. Several nanomicelle-like structures can be observed in Fig. 6c, and once more, we were able to identify grouped OA-IONPs at

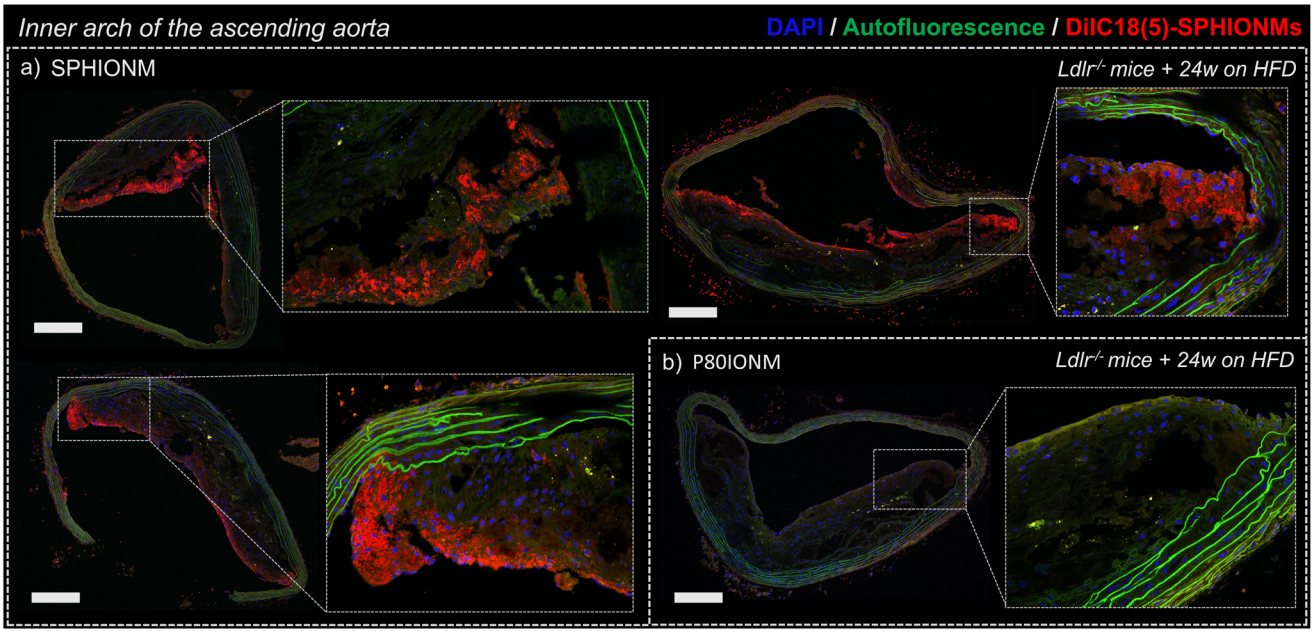

Fig. 5 *Ex vivo* confocal microscopy of SPHIONM accumulation in atherosclerotic lesions. Representative confocal microscopy images of sections of the inner arch of the ascending aorta of *Ldlr*$^{-/-}$ mice fed an HFD for 24 weeks and injected with (a) fluorescent SPHIONM (150 μL) (N = 5); (b) fluorescent control P80IONMs (150 μL) (N = 4). DAPI (blue), autofluorescence (green), and DiIC18(5)-SPHIONM (red) staining. Scale bars 200 μm.

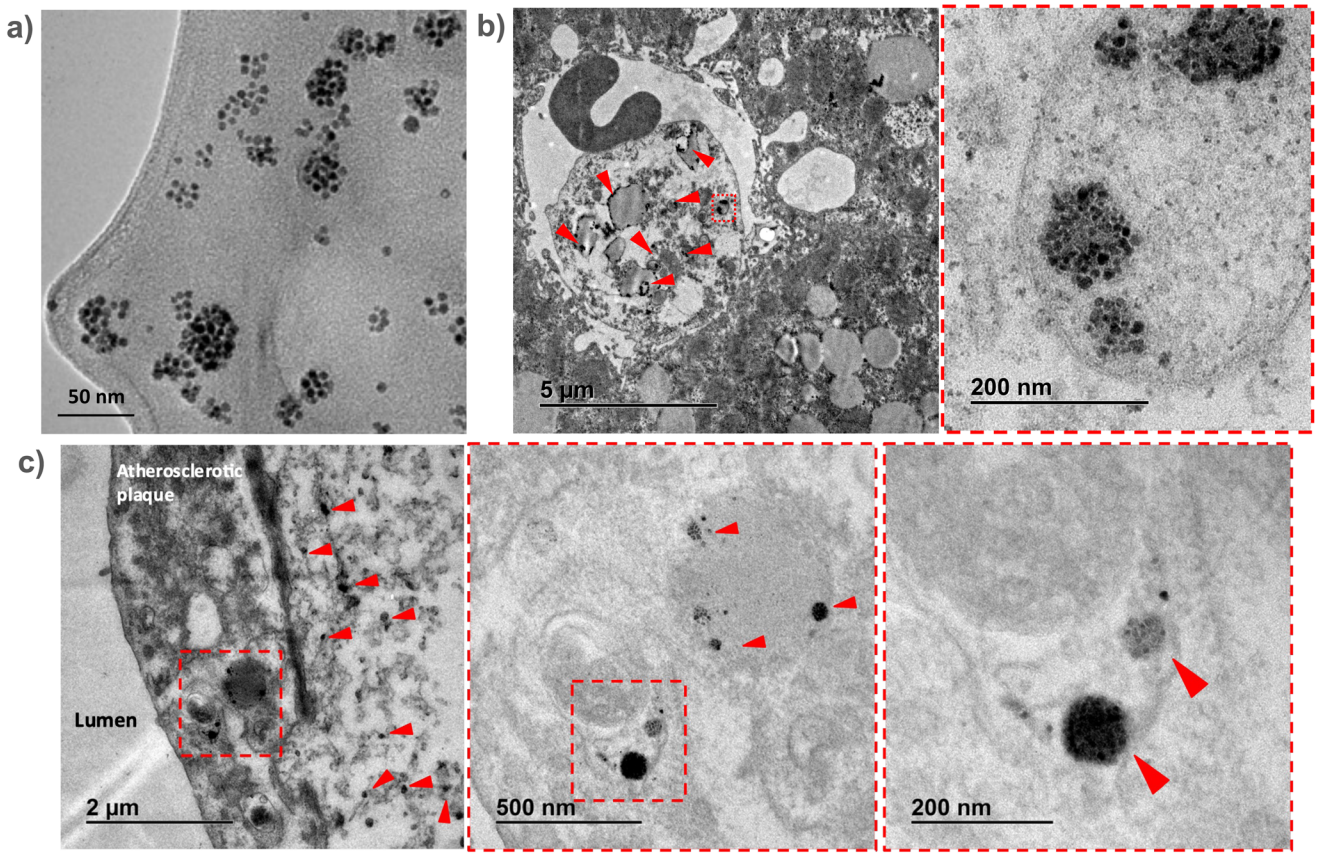

Fig. 6 *Ex vivo* analysis of SPHIONM accumulation in atherosclerotic lesions using TEM. Representative TEM images of tissue sections from atherosclerotic *Ldlr*$^{-/-}$ mice fed a HFD for 24 weeks and injected with SPHIONMs (150 µL) 24 h before euthanasia. (a) TEM images of SPHIONM solution; scale bar = 50 nm. (b) TEM images of a liver section; higher magnification of the same section (right); scale bars, 5 µm and 200 nm. Examples of accumulated SPHIONMs are marked with red arrows. (c) TEM images of a section of the inner arch of the ascending aorta; higher-magnification images of the same atherosclerotic plaque section (middle and right); scale bars, 2 µm, 500 nm, and 200 nm, respectively. The accumulated SPHIONMs are highlighted with red arrows.

higher magnifications. These results further corroborated the presence of SPHIONMs in the atherosclerotic plaque of *Ldlr*$^{-/-}$ mice, thus reinforcing the hypothesis that the signal changes in T_2-weighted MRI studies were due to their presence.

Colocalisation studies between SPHIONMs and sphingomyelinase

Finally, after demonstrating the ability of SPHIONMs to accumulate in atherosclerotic lesions, we aimed to address our hypothesis that arterial SMase participates in the nanomicelle aggregation process. For this purpose, the colocalisation of SMase and SPHIONMs was analysed in sections of plaque from *Ldlr*$^{-/-}$ mice fed a HFD for 24 weeks and injected with fluorescent SPHIONMs. Acid sphingomyelinase (SMPD1), a type of sphingomyelinase implicated in LDL retention[11] was stained by immunofluorescence using anti-SMPD1 and an Alexa Fluor 568-conjugated secondary antibody, and the distribution of the signal was compared to the fluorescence (DiIC18(5)) from accumulating SPHIONMs. SMPD1 distribution was observed in both control mice (Fig. 7a) and SPHIONM-injected mice, eliminating the possibility of colocalisation due to cross-contamination between fluorescence channels.

The fluorescent patterns displayed in the acquired confocal microscopy images showed clear colocalisation between SMase and SPHIONMs (Fig. 7b and d). The SMPD1 signal was higher in the plaque shoulders and in the middle part of the plaque close to the lumen, thus matching the previously observed SPHIONM signal pattern. In addition, to better visualise the patterns of each signal and their degree of colocalisation, signal masks were created from both the SMase and SPHIONMs fluorescence channels (Fig. 7c and e). To this end, an automatic intensity threshold and closing filter were applied to the original confocal microscopy signal. The obtained masks were then merged, resulting in colocalisation areas appearing in yellow. The merged images showed that SPHIONMs accumulated mainly in regions that were also positive for SMPD1. The colocalised regions were mainly present in the luminal regions of plaques, while the less intense SMPD1-positive regions deeper in the plaque typically did not co-localise with SPHIONMs.

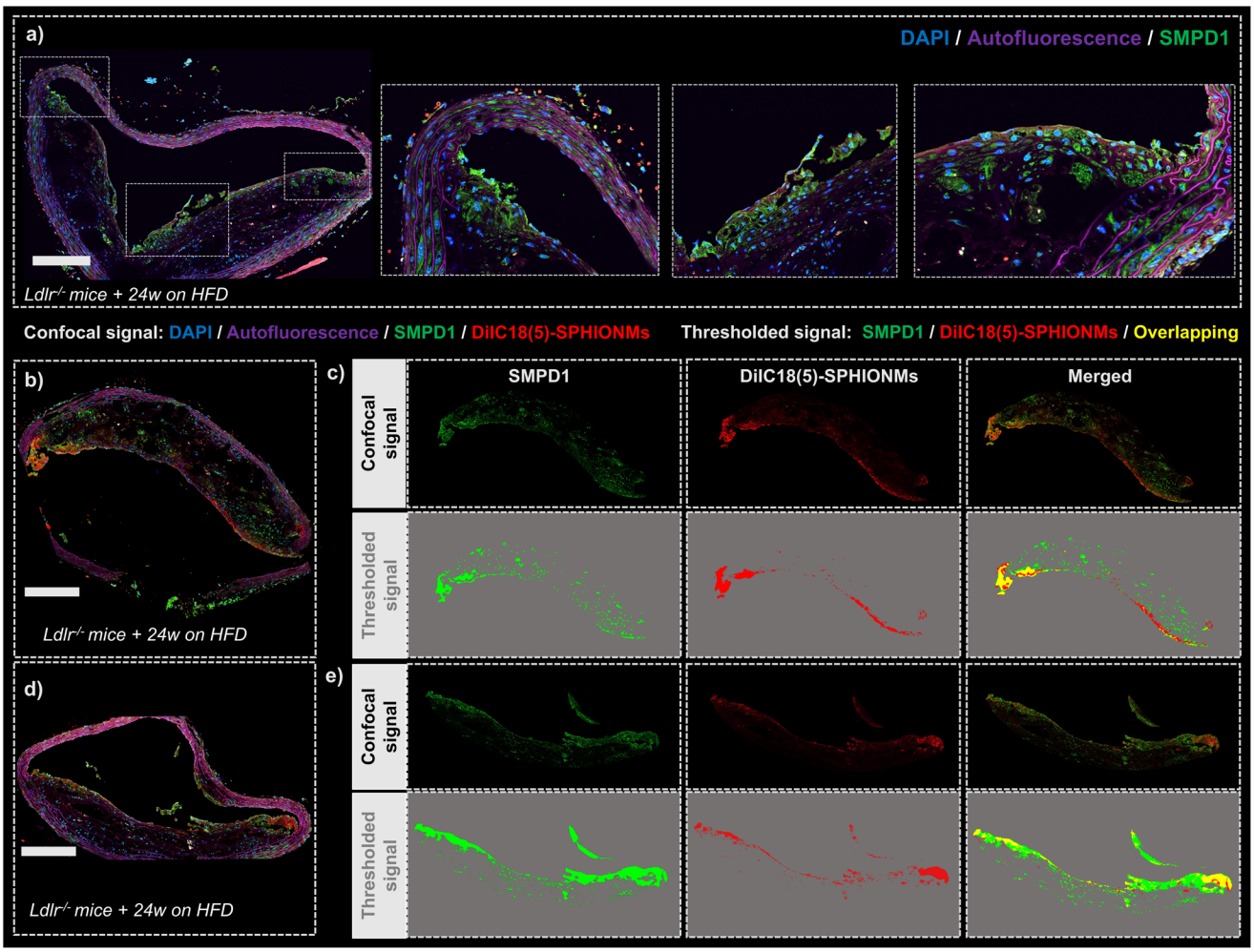

Fig. 7 Colocalisation of SPHIONMs and arterial SMase. (a) Representative confocal microscopy image of a section of the inner arch of the ascending aorta of an *Ldlr*$^{-/-}$ control mouse fed for 24 W with HFD and stained with an anti-SMPD1 primary antibody followed by an Alexa Fluor 568 conjugated secondary antibody. (b and d) Representative confocal microscopy images of sections of the inner arch of the ascending aorta of *Ldlr*$^{-/-}$ mice fed for 24 W with HFD and injected with fluorescent SPHIONMs (150 μL) (red). Sections were stained with an anti-SMPD1 primary antibody, followed by an Alexa Fluor 568 conjugated secondary antibody (green) for localisation of sphingomyelinase in the atherosclerotic plaque. (c and e) Panels representing the colocalisation between SMase and SPHIONM using the plaque signals from (b) and (d), respectively. The top panels show the real confocal signal from the SMPD1 channel, SPHIONM channel, and both channels merged (left to right); the autofluorescence signal was subtracted from all channels. Bottom panels show a signal mask of the signal of the SMPD1 channel (green), SPHIONM channel (red), and both merged (left to right). The overlapping mask signal is indicated in yellow. DAPI for nuclei staining appears dark blue and autofluorescence in magenta. All scale bars 200 μm.

Discussion

Sphingomyelin iron oxide nanomicelles (SPHIONMs), formed by a core of grouped hydrophobic iron oxide nanoparticles (IONPs) stabilised by sphingomyelin (SPH) molecules, were successfully developed in this study. These nanomicelles were designed to take advantage of SMase presence in the plaque and its ability to modify the zwitterionic head of SPH that provides colloidal stability to SPHIONMs. This process is key to our approach of imitating LDL aggregation in the plaque, especially considering the high susceptibility of SPH-enriched LDLs to aggregation within atherosclerotic plaques.[11,12] We were able to produce nanomicelles showing good colloidal (stability, size, and surface charge) and magnetic properties (high r_2/r_1 ratio), while obtaining high nanoparticle accumulation in atherosclerotic lesions, as demonstrated by MRI and confocal microscopy.

Our results showed that the SPHIONMs maintained their colloidal properties with high stability. Moreover, transmission electron microscopy (TEM) and thermogravimetric analysis (TGA) results showed that SPHIONMs have a nanomicelle-like structure with a similar core size and a thin layer of organic material at their surface. In addition, the measured relaxivities indicated that the ability to produce contrast on T_2-weighted MRI was maintained. Liver T_2-weighted MR images of mice injected with SPHIONMs showed a darkening effect that

increased with time, indicating that the nanomicelles circulated for at least 90 min. This demonstrated that they were not immediately eliminated by the RES system, which is important for their ability to enter and be retained in atherosclerosis. In addition, these results confirmed that the hypointense effect produced by the SPHIONMs was comparable to that of other superparamagnetic nanoparticles.[18]

Once we confirmed the optimal colloidal and magnetic properties of SPHIONMs, we demonstrated that they were susceptible to SMase action and that this enzymatic activity appeared to be responsible for their aggregation *in vivo*. The biological behaviour of nanoparticles may be altered upon exposure to biological fluids due to the formation of a protein corona, a layer of proteins that adsorb onto the surface of nanoparticles, capable of altering their surface properties.[19] In SPHIONMs, the protein corona could have hindered the ability of SMase to reach the polar heads of the sphingomyelin molecules, thus preventing their retention within atherosclerotic lesions. However, immunohistochemistry studies showed colocalisation between nanomicelle accumulation and SMase in the luminal regions of plaque, suggesting, albeit not proving, that the SPHIONMs did not lose their ability to be responsive to the specific enzymatic action. In addition, confocal microscopy studies showed that SPHIONMs preferentially bind to the plaque shoulder of aortic arch sections. The shoulder is a predilection site for inflammation, potentially driven by incoming LDLs; hence, its permeability for the NPs might be increased, allowing a higher number through when compared to other regions of the plaque. Furthermore, as we observed, the shoulder is a region with extensive SMase expression, which favours nanomicelle aggregation. Finally, the shoulder region is also the most vulnerable to plaque rupture;[20] hence, the high accumulation of nanoparticles in this region suggests that SPHIONMs could potentially be used for the identification of high-risk plaques.

One of the goals for developing SPHIONMs was to use them as molecular imaging probes for atherosclerosis visualisation using MRI. Iron oxide nanoparticles represent a potentially safe class of molecular probes for translational imaging compared to Gd-containing contrast agents, which have been shown to have significant toxicity in conditioned or diseased patients, most importantly in patients with renal dysfunction.[21] However, high doses of iron may also produce toxic effects.[22] Compared to other nanoparticles used for the targeted detection of atherosclerosis using T_2-weighted MRI, SPHIONMs presented a low iron concentration of 0.38 mg mL^{-1}. Adjusted to the injected volumes (150–200 μL), this concentration was equivalent to injecting approximately 2 mg Fe per kg, compared with the 5–12 mg Fe per kg normally injected.[18,23–25] This low concentration was proven to be sufficient to produce changes in the contrast of the MR images in a similar manner to those shown in previous studies.[18,23,26]

Results from T_2-weighted MRI studies in $Ldlr^{-/-}$ mice showed changes in the aortic wall signal after the injection of the nanomicelles, which were not observed after the injection of control (P80IONM) nanomicelles. Even if T_2-weighted images must be taken with caution, since they may present several limitations that may hinder signal quantification, results observed in Fig. 4 clearly indicate the accumulation of SPHIONMs in the arterial wall. Images show a negative contrast in the arterial wall after SPHIONMs injection that is not present when using control nanomicelles. Signal quantification in MRI, particularly using negative contrast, can be difficult. The intensity measured within the ROIs manually drawn over the arterial wall before and after nanomicelle injection, showed that differences between baseline and post-injection intensities were only observed in those mice injected with the SPHIONMs. Although T_2-weighted MR images should show a signal decrease with superparamagnetic contrast agents, the presence of magnetic nanoparticles, such as SPHIONMs, in the field of view will increase the magnetic susceptibility of the area, which can result in the scattered intensity values that we measured.[27]

Conclusions

In this study, we successfully demonstrated the use of enzymatic activity in the plaque to develop a nanoplatform capable of accumulating in atherosclerotic lesions. This molecular imaging probe, sphingomyelin iron oxide nanomicelles (SPHIONMs), was synthesised using a reproducible method that yields colloidally stable nanomicelles suitable for T_2-weighted MRI. SPHIONMs were capable of accumulating in established murine atherosclerotic plaques as shown by T_2-weighted MRI *in vivo* experiments, and confocal microscopy and TEM *ex vivo* experiments. In addition, immunohistochemistry studies showed colocalisation between nanomicelle accumulation and SMase in the luminal regions of plaque, suggesting that the SMase enzymatic action contributes to the aggregation process.

Author contributions

J. F. B. and F. H. designed, analysed the experiments and wrote the manuscript. M. M.-H. performed the experimental work and wrote the manuscript. P. N., I. F.-B. and J. R.-C. performed the experimental work. All authors have read and agreed to the publication of this manuscript.

Conflicts of interest

There are no conflicts to declare.

Acknowledgements

This study was supported by grants from the Ministerio de Economía, Industria y Competitividad (MEIC) with cofunding from the European Regional Development Fund (PID2019-108568RB-I00) and Ministerio de Ciencia e Innovación (PID2019-104059RB-100, PDC2022-133493-100, RED2022-134299-T), Comunidad de Madrid (P2022/BMD-7333) and La

Caixa Health Research Programme (HR20-00075, AtheroConvergence). CNIC is supported by the Instituto de Salud Carlos III (ISCIII), the Ministerio de Ciencia e Innovación (MCIN) and the Pro CNIC Foundation, and is a Severo Ochoa Center of Excellence (grant CEX2020-001041-S funded by MICIN/AEI/10.13039/501100011033).

References

1 M. L. Senders, S. Hernot, G. Carlucci, J. C. van de Voort, F. Fay, C. Calcagno, J. Tang, A. Alaarg, Y. Zhao, S. Ishino, A. Palmisano, G. Boeykens, A. E. Meerwaldt, B. L. Sanchez-Gaytan, S. Baxter, L. Zendman, M. E. Lobatto, N. A. Karakatsanis, P. M. Robson, A. Broisat, G. Raes, J. S. Lewis, S. Tsimikas, T. Reiner, Z. A. Fayad, N. Devoogdt, W. J. M. Mulder and C. Pérez-Medina, *JACC Cardiovasc. Imaging*, 2019, **12**, 2015–2026.

2 M. Nahrendorf, E. Keliher, B. Marinelli, F. Leuschner, C. S. Robbins, R. E. Gerszten, M. J. Pittet, F. K. Swirski and R. Weissleder, *Arterioscler., Thromb., Vasc. Biol.*, 2011, **31**, 750–757.

3 J. Pellico, I. Fernández-Barahona, J. Ruiz-Cabello, L. Gutiérrez, M. Muñoz-Hernando, M. J. Sánchez-Guisado, I. Aiestaran-Zelaia, L. Martínez-Parra, I. Rodríguez, J. Bentzon and F. Herranz, *ACS Appl. Mater. Interfaces*, 2021, **13**, 45279–45290.

4 J. Pellico, I. Fernández-Barahona, M. Benito, Á. Gaitán-Simón, L. Gutiérrez, J. Ruiz-Cabello and F. Herranz, *Nanomedicine*, 2019, **17**, 26–35.

5 K. A. Kelly, J. R. Allport, A. Tsourkas, V. R. Shinde-Patil, L. Josephson and R. Weissleder, *Circ. Res.*, 2005, **96**, 327–336.

6 J. Talev and J. R. Kanwar, *Semin. Thromb. Hemostasis*, 2020, **46**, 553–562.

7 P. Libby, P. M. Ridker and G. K. Hansson, *Nature*, 2011, **473**, 317–325.

8 K. J. Williams and I. Tabas, *Arterioscler., Thromb., Vasc. Biol.*, 1995, **15**, 551–561.

9 I. Tabas, Y. Li, R. W. Brocia, S. W. Xu, T. L. Swenson and K. J. Williams, *J. Biol. Chem.*, 1993, **268**, 20419–20432.

10 Z. Yu, Q. Peng and Y. Huang, *Clin. Sci.*, 2019, **133**, 763–776.

11 C. M. Devlin, A. R. Leventhal, G. Kuriakose, E. H. Schuchman, K. J. Williams and I. Tabas, *Arterioscler., Thromb., Vasc. Biol.*, 2008, **28**, 1723–1730.

12 M. Ruuth, S. D. Nguyen, T. Vihervaara, M. Hilvo, T. D. Laajala, P. K. Kondadi, A. Gisterå, H. Lähteenmäki, T. Kittilä, J. Huusko, M. Uusitupa, U. Schwab, M. J. Savolainen, J. Sinisalo, M.-L. Lokki, M. S. Nieminen, A. Jula, M. Perola, S. Ylä-Herttula, L. Rudel, A. Öörni, M. Baumann, A. Baruch, R. Laaksonen, D. F. J. Ketelhuth, T. Aittokallio, M. Jauhiainen, R. Käkelä, J. Borén, K. J. Williams, P. T. Kovanen and K. Öörni, *Eur. Heart J.*, 2018, **39**, 2562–2573.

13 Y. Ma, W. Wang, J. Zhang, Y. Lu, W. Wu, H. Yan and Y. Wang, *PLoS One*, 2012, **7**, e35835.

14 A. V. Lechuga-Vieco, H. Groult, J. Pellico, J. Mateo, J. A. Enríquez, J. Ruiz-Cabello and F. Herranz, *Nanomedicine*, 2018, **14**, 643–650.

15 J. Ibarra, J. Melendres, M. Almada, M. G. Burboa, P. Taboada, J. Juárez and M. A. Valdez, *Mater. Res. Express*, 2015, **2**, 095010.

16 F. Herranz, M. P. Morales, A. G. Roca, M. Desco and J. Ruiz-Cabello, *Chem. – Eur. J.*, 2008, **14**, 9126–9130.

17 V. Peiffer, S. J. Sherwin and P. D. Weinberg, *Cardiovasc. Res.*, 2013, **99**, 242–250.

18 S. Wen, D.-F. Liu, Y. Cui, S. S. Harris, Y. Chen, K. C. Li, S. Ju and G.-J. Teng, *Nanomedicine*, 2014, **10**, 639–649.

19 S. Tenzer, D. Docter, J. Kuharev, A. Musyanovych, V. Fetz, R. Hecht, F. Schlenk, D. Fischer, K. Kiouptsi, C. Reinhardt, K. Landfester, H. Schild, M. Maskos, S. K. Knauer and R. H. Stauber, *Nat. Nanotechnol.*, 2013, **8**, 772–781.

20 U. Beisiegel, W. Weber, G. Ihrke, J. Herz and K. K. Stanley, *Nature*, 1989, **341**, 162–164.

21 M. A. Perazella, *Clin. J. Am. Soc. Nephrol.*, 2009, **4**, 461–469.

22 B. Szalay, E. Tátrai, G. Nyírő, T. Vezér and G. Dura, *J. Appl. Toxicol.*, 2012, **32**, 446–453.

23 K. C. Briley-Saebo, Y. S. Cho, P. X. Shaw, S. K. Ryu, V. Mani, S. Dickson, E. Izadmehr, S. Green, Z. A. Fayad and S. Tsimikas, *J. Am. Coll. Cardiol.*, 2011, **57**, 337–347.

24 F. Yan, W. Yang, X. Li, H. Liu, X. Nan, L. Xie, D. Zhou, G. Xie, J. Wu, B. Qiu, X. Liu and H. Zheng, *BioMed Res. Int.*, 2015, **2015**, 1–10.

25 M.-J. Jacobin-Valat, K. Deramchia, S. Mornet, C. E. Hagemeyer, S. Bonetto, R. Robert, M. Biran, P. Massot, S. Miraux, S. Sanchez, A.-K. Bouzier-Sore, J.-M. Franconi, E. Duguet and G. Clofent-Sanchez, *NMR Biomed.*, 2011, **24**, 413–424.

26 K. Morishige, D. F. Kacher, P. Libby, L. Josephson, P. Ganz, R. Weissleder and M. Aikawa, *Circulation*, 2010, **122**, 1707–1715.

27 M. A. Busquets, J. Estelrich and M. J. Sánchez-Martín, *Int. J. Nanomed.*, 2015, **10**, 1727.